Chemistry
A European
Journal

Chemistry Europe
European Chemical Societies Publishing

Accepted Article

Title: The Most Active Oxidase-mimicking Mn2O3 Nanozyme for Biosensor Signal Generation

Authors: Zi-Jian Chen, Zhicheng Huang, Yuan-Ming Sun, Zhen-Lin Xu, and Juewen Liu

To be cited as: *Chem. Eur. J.* 10.1002/chem.202100567

Link to VoR: https://doi.org/10.1002/chem.202100567

WILEY-VCH

10.1002/chem.202100567

The Most Active Oxidase-mimicking Mn_2O_3 Nanozyme for Biosensor Signal Generation

Zi-Jian Chen[1,2], Zhicheng Huang[2], Yuan-Ming Sun[1], Zhen-Lin Xu[1]* and Juewen Liu[2]*

Dr. Zi-Jian Chen, Prof. Yuan-Ming Sun and Prof. Zhen-Lin Xu

1. Guangdong Provincial Key Laboratory of Food Quality and Safety, South China Agricultural University, Guangzhou 510642, China.

Email: jallent@163.com

Dr. Zi-Jian Chen, Zhicheng Huang and Prof. Juewen Liu

2. Department of Chemistry, Waterloo Institute for Nanotechnology, University of Waterloo, Waterloo, Ontario, N2L 3G1, Canada

Email: liujw@uwaterloo.ca

Twitter: @bionaloo

10.1002/chem.202100567

Abstract

Oxidase-mimicking nanozymes are more desirable than peroxidase-mimicking ones since H_2O_2 can be omitted. However, only a few nanomaterials are known for oxidase-like activities. In this work, we compared the activity of Mn_2O_3, Mn_3O_4 and MnO_2 and found that Mn_2O_3 had the highest oxidase activity. Interestingly, the activity of Mn_2O_3 was even inhibited by H_2O_2. The oxidase-like activity of Mn_2O_3 was not much affected by the presence of proteins such as bovine serum albumin (BSA), but the physisorption of antibodies to Mn_2O_3 was not strong enough to withstand the displacement by BSA. We then reacted Mn_2O_3 with 3-aminopropyltriethoxysilane to graft an amine group, which was used to conjugate antibodies using glutaraldehyde as a crosslinker. A one-step indirect competitive ELISA (icELISA) was developed for the detection of isocarbophos, and an IC_{50} of 261.7 ng/mL was obtained, comparable with the results of the standard two-step assay using horseradish peroxidase (HRP)-labeled antibodies. This assay has the advantage of significant timesaving attractive for rapid detection of large amounts of samples. This work has discovered a highly efficient oxidase-mimicking nanozyme useful for various nano and analytical applications.

Keywords: nanozymes; catalysis; manganese oxide; immunoassays; antibodies

Introduction

With high stability and low cost, nanozymes[1-4] are promised to replace horseradish peroxidase (HRP) in biosensors, especially in immunoassays.[5-8] So far, many peroxidase-mimicking nanozymes have been developed, such as Fe_3O_4,[5, 9, 10] Pd-Ir,[11] Pd@Pt,[12, 13] Pd@Au,[14] and MnO_2.[15, 16] However, unstable H_2O_2 is required. In this regard, oxidase-mimicking nanozymes are more attractive, which can directly use molecular oxygen as an oxidant. Metal oxide nanoparticles are a great source of oxidase-mimicking nanozymes. CeO_2 nanoparticles are a representative example, but its activity is low and fluoride can be added to boost the activity.[17-21] NiO is another oxidase mimic but it can only use Amplex red as a substrate. Hence, a general and highly active oxidase-like nanozyme is still in need.

Manganese has rich oxidation states, and its oxides exhibit various enzyme-like activities. MnO_2[15, 16, 22, 23] and Mn_3O_4[24-26] nanoparticles with peroxidase or oxidase-like activities have been reported. Furthermore, Mugesh and coworkers reported that Mn_3O_4 has superoxide dismutase, catalase and glutathione peroxidase activities.[27] Mn_2O_3 was reported to have peroxidase,[28] and glucose oxidase (GOx)-like activity.[29] A systematic comparison of the oxidase-like activity of manganese oxides is still lacking.

Organophosphorus pesticides (OPs) are widely used due to their excellent efficacy and relatively rapid degradation.[30-32] However, residual OPs are harmful to human beings and the environment. Instrumental analysis of OPs is limited by the high cost and long

turnaround time.[33-35] For rapid and on-site detection, immunoassays are an attractive alternative.[36-40] Herein, we compared the activities of various manganese oxide nanoparticles and found that Mn_2O_3 nanoparticles had the highest oxidase-mimicking activity among them. We then used the Mn_2O_3 nanozyme to develop a one-step ELISA for the rapid detection of isocarbophos, an important OP.

Materials and methods

Chemicals

The isocarbophos and analogue standards were purchased from Tanmo Reference Material Technology Ltd. (Beijing, China). Isopropyl salicylate and 4-aminobutyric acid were obtained from Heowns Biochemical Technology co. Ltd. (Tianjin, China). 3,3',5,5'-Tetramethylbenzidine (TMB), 2,2'-azino-bis(3-ethylbenzothiazoline-6-sulfonic acid) (ABTS), dopamine, Amplex red, hydrogen peroxide (30 wt%), (3-aminopropyl)-triethoxysilane (APTES), cerium (IV) oxide (dispersed in 2.5% acetic acid), and FITC-BSA were obtained from Sigma-Aldrich. Fe_3O_4, Co_3O_4, CoO, Mn_2O_3, Mn_3O_4 and NiO nanoparticles were purchased from US Research Nanomaterials, Inc. 4-(2-hydroxyethyl)piperazine-1-ethanesulfonate (HEPES) was from Mandel Scientific (Guelph, Ontario, Canada). The PBS buffer contained 10 mM phosphate and 75 mM NaCl. The PBST (PBS with 0.05% Tween 20) buffer was prepared by adding Tween 20 to the PBS

buffer.

Preparation of anti-isocarbophos monoclonal antibody (mAb)

The details of hapten synthesis and characterization (Figure S1-S3), artificial antigen synthesis and characterization (Figure S4 and S5), animal immunization (Figure S6, Table S1), anti-isocarbophos monoclonal antibody (anti-ISO mAb) preparation and isotyping of mAb (Figure S7) are showed in Supporting Information.

Comparison of the activity of different nanozymes

In general, the metal oxide nanoparticles (10 μg/mL, 1 mL) were incubated with TMB (0.5 mM, in 50 mM pH 4.0 acetate buffer) with or without H_2O_2 (20 mM) for 1 min reaction. To investigate the oxidase-like activity of Mn_2O_3, TMB (0.5 mM), ABTS 0.5 mM), dopamine (1 mM) and Amplex red (1 μM) were applied as substrates. For studying the catalytic parameters, Mn_2O_3 (2.5 μg/mL) was used to catalyze various concentrations of TMB. The UV-vis absorbance, A, was then converted to concentrations c, through Beer's law: $A = \varepsilon cl$ (ε= 39000 and 36800 M^{-1} cm^{-1} for TMB and ABTS, respectively, and l is the optical pathlength of 1 cm). To study the effect of buffer, Mn_2O_3 (100 μg/mL, 5 μL) was mixed with 100 μL 0.5 mM TMB in different buffers (50 mM, pH 4.0) for 30 min kinetic study (absorbance monitored at 652 nm). To study the effect of H_2O_2 concentration on Mn_2O_3 activity, Mn_2O_3 (1 mg/mL, 1 μL) was mixed with 100 μL TMB (0.5 mM) in acetate buffer (50 mM, pH 4.0) for 2 min reaction with various concentrations of H_2O_2, and the

absorbance was measured at 652 nm.

Effect of protein on the activity of nanozyme

The metal oxide nanoparticles (2 mg/mL, 500 μL) were respectively incubated with various concentration of BSA for 1 h. Each protein-capped nanozyme (4 μL) was mixed with 400 μL of substrate and subsequently the mixtures were reacted for 1 h. For the peroxidase-like nanozymes, 0.5 mM TMB and 20 mM H_2O_2 in acetate buffer (50 mM, pH 4.0) were applied. For reaction conditions of the oxidase-like nanozymes are summarized in Table S2.

Protein and antibody adsorption by nanozymes

To study the adsorption of proteins by nanozymes, the metal oxide nanoparticles (2 mg/mL, 500 μL) were incubated with FITC-BSA (200 μg/mL) for 0.5 h, or with the anti-isocarbophos antibody (20 μg/mL) for 2 h. The mixtures were then centrifuged (15000 rpm, 10 min) and the fluorescence intensity of supernatant was measured (Ex 490 nm; Em 535 nm). To study the desorption of the proteins from nanozymes, all the nanozymes were divided into two tubes (200 μL); one was added with 5 μL of BSA (100 mg/mL) and the other with 5 μL H_2O. To desorb FITC-BSA, 0.5 h incubation was used, and the fluorescence in the supernatants was measured after centrifugation (15000 rpm, 10 min). To desorb the antibody, 2 h incubation was used, and the supernatant was 1000-fold diluted for titer measurement by icELISA.

Preparation of antibody-conjugated Mn_2O_3@APTES

Mn_2O_3 (50 mg) was dispersed in 10 mL of 50% ethanol and then 250 μL of APTES was added with stirring. The mixture was stirred for another 12 h at 60 ℃ and washed by H_2O for twice after the reaction to prepare Mn_2O_3@APTES. Then, 500 μL Mn_2O_3@APTES (3.6 mg/mL), 100 μL MES buffer (500 mM, pH 6.0) and 400 μL glutaraldehyde (25%) were mixed and stirred overnight in dark. Afterwards, the mixture was washed by H_2O three times. Then, 1 mL MES buffer (50 mM) and 10 μL monoclonal antibody (8.5 mg/mL) were added and stirred for 2 h at room temperature in dark. After that, 20 μL BSA (100 mg/mL) was added to block the nonspecific adsorption sites for 2 h. The blocked Mn_2O_3@APTES was centrifuged and re-dispersed in 10 mM PBS (pH7.4). Finally, 100 μL of freshly prepared sodium borohydride (4 mg/mL) was added and stirred for 1 h in dark, and the sample was subsequently washed by PBS for three times. The obtained antibody-conjugated Mn_2O_3@APTES was dissolved in PBS with a final concentration of 3.2 mg/mL.

Immunoassays

The one-step indirect competitive ELISA (icELISA) was developed based on the Mn_2O_3@APTES conjugated antibody. Briefly, 50 μL of PBS or competitor was added to each well and 50 μL of Mn_2O_3@APTES-labeled mAb was then added and incubated at 37 ℃ for 40 min. After incubation, the plate was washed five times with PBST. Then 100 μL TMB (1 mM) was added and reacted at 37 ℃ for 10 min, while the absorbance was measured at 450 nm after 50 μL/well of 10% H_2SO_4 was added. The ELISA calibration

curve was obtained by plotting the percent binding of antibodies in the wells (B/B_0) against the logarithm of the target concentration. The 50% decrease in A_{max} (IC_{50}) was calculated. For comparison, the conventional two-step icELISA was also applied for isocarbophos. After the same incubation step, the plate was washed five times with PBST. Then, 100 μL of HRP-conjugated goat anti-mouse secondary antibody (2000-fold diluted by PBST) was added to each well for 30 min incubation at 37 ℃. After 5 times washing by PBST, 100 μL of 5 mM TMB (in 20 mM pH 4.0 citrate buffer, with 10 mM H_2O_2) was added to each well and incubated at 37 ℃ for 10 min. Finally, 50 μL of 10% H_2SO_4 was added to stop the activity of HRP and the absorbance was measured at 450 nm.

Recovery Test

Three levels of isocarbophos were added to 5.0 g samples (cucumber and Chinese cabbage) and extracted by 5 mL acetonitrile and vortexed to extract isocarbophos for 2 min. Then Na_2SO_4 (2 g) was added and vortexed for 2 min to remove water. The mixture was centrifuged at 4000 rpm for 10 min. 1 mL of supernatant was dry by nitrogen flow at 65 ℃ and re-dissolved by 1 mL of 10 mM PBS. The re-dissolved solution was diluted and then applied for the ELISA test.

Results and Discussion

Mn_2O_3 as a highly active oxidase-mimicking nanozyme

10.1002/chem.202100567

We first compared the oxidase and peroxidase-like activities of three types of manganese oxides: MnO_2, Mn_3O_4, and Mn_2O_3. Their TEM micrographs showed spherical particles of around 35 nm, 58 nm, and 60 nm, respectively (Figure 1A-C). XRD confirmed their crystalline structures (Figure 1D). Dynamic light scattering showed the largest hydrodynamic size of Mn_2O_3 among them reaching over 300 nm, which was attributed to aggregation (Figure 1E). We also measured the ζ-potential at pH 4, 7.4 and 9 for them, and in general lower pH gave more positive potentials (Figure 1F). At neutral pH, all the manganese oxides were negatively charged. In addition, we also used CeO_2 nanoparticles of 5 nm for comparison (Figure 1E), which were close to charge neutral at neutral pH.

10.1002/chem.202100567

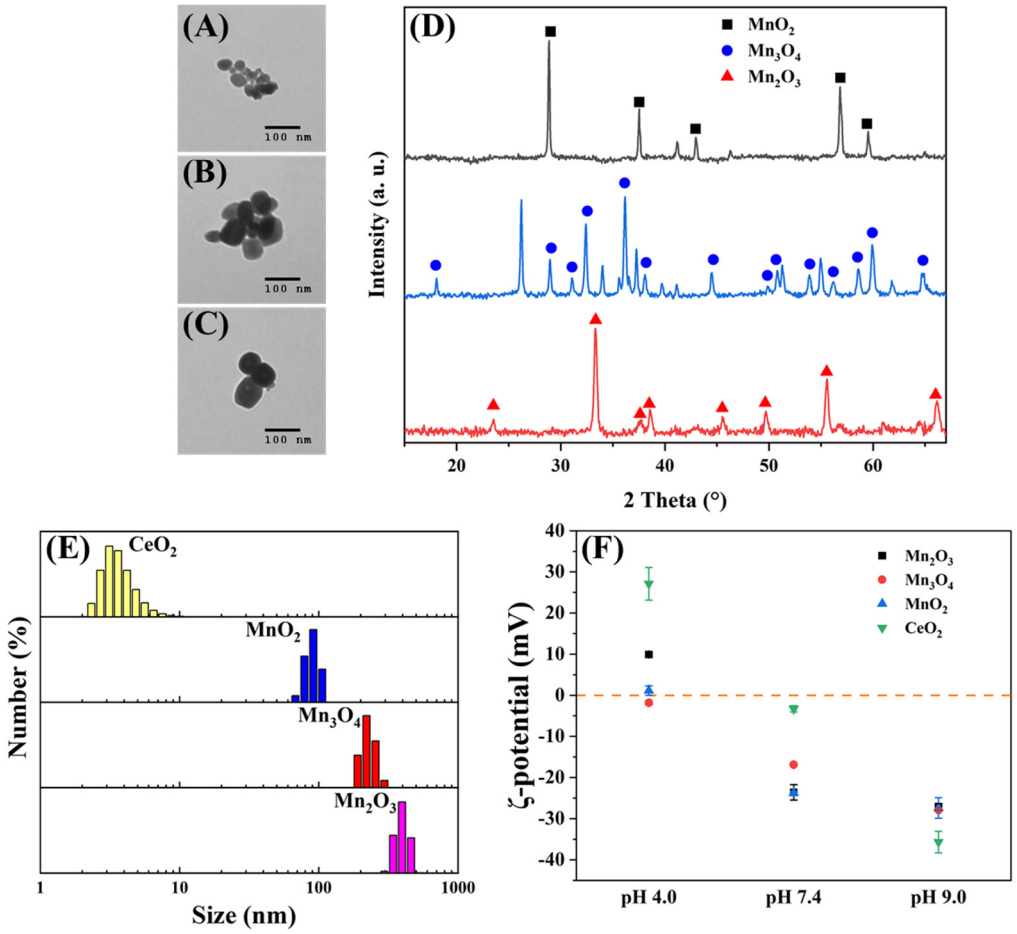

Figure 1. The TEM micrographs of the (A) MnO_2 (B) Mn_3O_4 and (C) Mn_2O_3 nanoparticles used in this work. (D) XRD spectra of the three manganese oxide nanoparticles. The diffraction peaks indicated by the symbols are ■MnO_2, ●Mn_3O_4 and ▲Mn_2O_3, respectively. (E) The hydrodynamic size and (F) ζ-potential of the manganese oxide and CeO_2 nanoparticles used in this work.

We then investigated the oxidase-like catalytic activity of different oxides using TMB as a substrate at pH 4.0, and Mn_2O_3 was much more active than the rest as judged from the

10.1002/chem.202100567

strongest blue color of oxidized TMB (Figure 2A, upper row). The activity followed Mn_2O_3 > MnO_2 > Mn_3O_4 > CeO_2, while the rest did not show much color change. Therefore, Mn_2O_3 is the most active oxidase-mimic that works under ambient conditions. To further confirm the activities, Mn_2O_3 dispersions in H_2O or in pH 4 buffer were centrifuged and the supernatants and pellets were respectively assayed with TMB. Blue color was observed only in the re-dispersed pellets (Figure 2B), suggesting that Mn_2O_3 was the source of activity instead of dissolved metal ions. Kinetic studies also confirmed the highest activity of Mn_2O_3 among them (Figure 2C). Based on the TEM and DLS data above, the Mn_2O_3 had the largest size among these three manganese oxides and thus its highest activity cannot be explained by the difference in specific surface area. To further confirm the surface area, the BET surface area of the three manganese oxide nanoparticles was also measured (Table S3). In the dried state, the Mn_2O_3 and Mn_3O_4 had a similar specific surface area, both of which were about 10-fold higher than that of the MnO_2. Therefore, the Mn_2O_3 did not have a distinct surface area advantage based on BET either. As a result, we reason that the Mn_2O_3 must have the highest intrinsic activity.

10.1002/chem.202100567

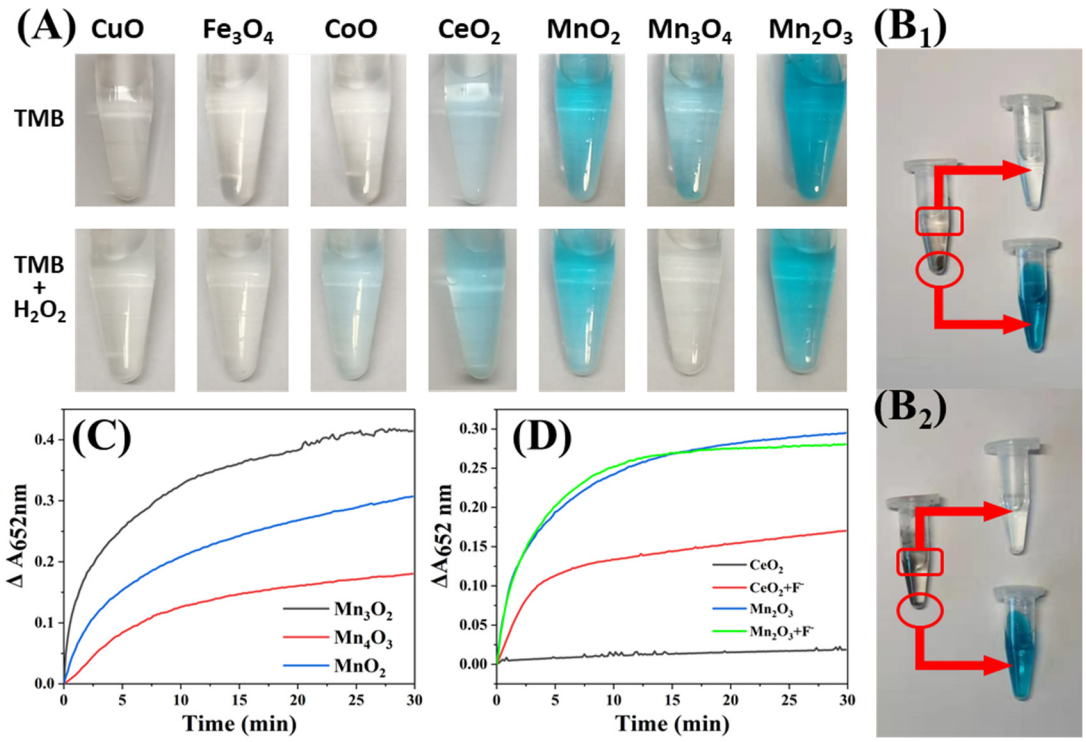

Figure 2. (A) Photographs showing the oxidase-like (upper row, no H_2O_2) and peroxidase-like (bottom row, 20 mM H_2O_2) activities of various metal oxide nanoparticles (10 μg/mL) for TMB (0.5 mM) in acetate buffer (50 mM, pH 4.0) after 1 min reaction. The oxidase-like activity of the supernatant and pellet of Mn_2O_3 (10 mg/mL) in water (B_1) and 50 mM pH4.0 acetate buffer (B_2). (C) Kinetics of oxidation of TMB with the three manganese oxides. (D) Kinetics of 0.5 mM TMB oxidation by Mn_2O_3 (10 μg/mL), CeO_2 (10 μg/mL) in the absence and presence of 3 mM F^- in pH 4.0 buffer.

Since CeO_2 is another commonly used oxidase nanozyme and F^- could boost its activity,[17-19] we also compared the activity of CeO_2 and Mn_2O_3 in the absence and

presence of F^-. Although the activity of CeO_2 was accelerated by F^-, its activity was still significantly lower than the bare Mn_2O_3 (Figure 2D). Mn_2O_3 had a similar activity regardless of F^-. It needs to be pointed out that the size of the CeO_2 was much smaller than that of Mn_2O_3, and they were tested at the same mass concentration. Thus, the oxidase-like activity of Mn_2O_3 was very strong.

To characterize the oxidase-mimicking activity of Mn_2O_3, we varied concentration of the TMB substrate and fitted the data using the Michaelis−Menten model (Figure S8). Good catalytic activity was observed with a V_{max} of 0.15 μM s^{-1}, and a K_m of 0.13 mM (100 μg/mL). For comparison, 100 μg/mL CeO_2 nanoparticles had a V_{max} of 0.07 μM s^{-1} and a K_m of 1.5 mM[19]. This quantitative comparison also indicated the high activity of Mn_2O_3.

We further investigated whether the Mn_2O_3 nanoparticles can catalyze other substrates. Figure 3A shows that ABTS, dopamine and Amplex red can also be oxidized, indicating a general oxidase-like activity of Mn_2O_3. The activity of Mn_2O_3 decreased as the pH increased (Figure 3B). Among the different buffers at pH 4, the acetate buffer gave the highest activity, although the citrate and phosphate buffer also worked quite well (Figure 3C). We also investigated the effect of salt concentration. While homogeneous blue color was observed without NaCl, aggregation was observed with more NaCl added (Figure S9).

10.1002/chem.202100567

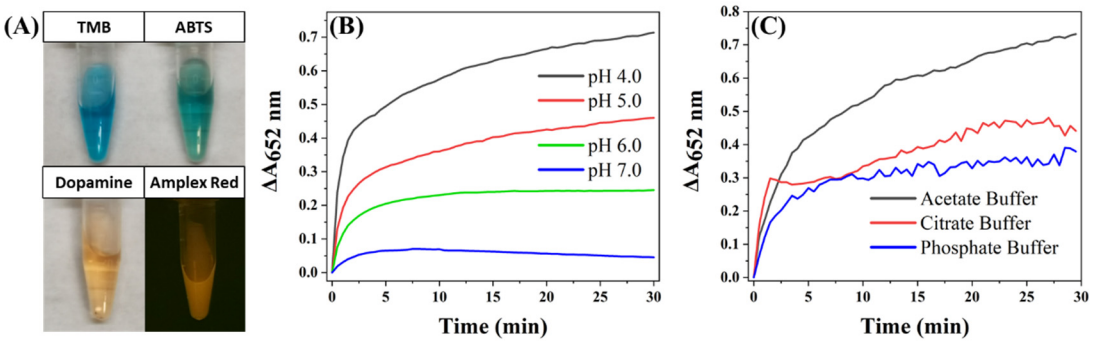

Figure 3. (A) Photographs showing the oxidase-like activity of Mn_2O_3 (10 μg/mL) to TMB (0.5 mM), ABTS (0.5 mM), dopamine (0.5 mM, with 100 μg/mL Mn_2O_3) and Amplex red (2 μM) at pH 4.0 after 10 min of reaction. (B) Effect of pH (50 mM acetate buffer) on the activity of Mn_2O_3 (10 μg/mL) to TMB (0.5 mM). (C) The effect of different buffer (pH 4, 50 mM) on the activity of Mn_2O_3 (5 μg/mL) for the oxidation of TMB.

Comparison of peroxidase-like activity

After understanding the oxidase-like activity, we then turned to the peroxidase reaction. In the bottom row of Figure 2A, the activity of most nanoparticles increased in the presence of H_2O_2, suggesting that they have stronger peroxidase-like activity. Interestingly, the activity of Mn_2O_3 and Mn_3O_4 was inhibited by H_2O_2. By titrating different concentrations of H_2O_2, Mn_2O_3 was inhibit with an apparent K_i (inhibition constant) of 21.2 mM H_2O_2 (Figure 4A and the red line in Figure 4B). Similarly, Mn_3O_4 had an apparent K_i of 0.14 mM H_2O_2 (black line and inset in Figure 4B). Therefore, Mn_3O_4 was much more strongly inhibited by H_2O_2. Even though the activity of MnO_2 was promoted by H_2O_2, it was still

10.1002/chem.202100567

weaker than the H_2O_2 inhibited activity of Mn_2O_3 (Figure 3D).

When reacting with H_2O_2, we observed a lot of gas bubbles from MnO_2 and a few from Mn_2O_3, while Mn_3O_4 had almost no bubble (Figure 3C). The amount bubbles reflected the decomposition of H_2O_2 into water and O_2. Mn_2O_3 has exclusive Mn^{3+}, MnO_2 has exclusively Mn^{4+}, while Mn_3O_4 has a mixture of Mn^{2+} and Mn^{3+}. Therefore, it seems that the activity was performed by Mn^{3+}.[41] This is understandable since Mn^{3+} is a strong oxidant,[41] whereas Mn^{2+} is a stable ion without strong oxidation activity. H_2O_2 can oxidize the Mn^{3+} species into Mn^{4+} or reduce it to Mn^{2+}. Either way, the oxidase-like activity would be decreased by H_2O_2.

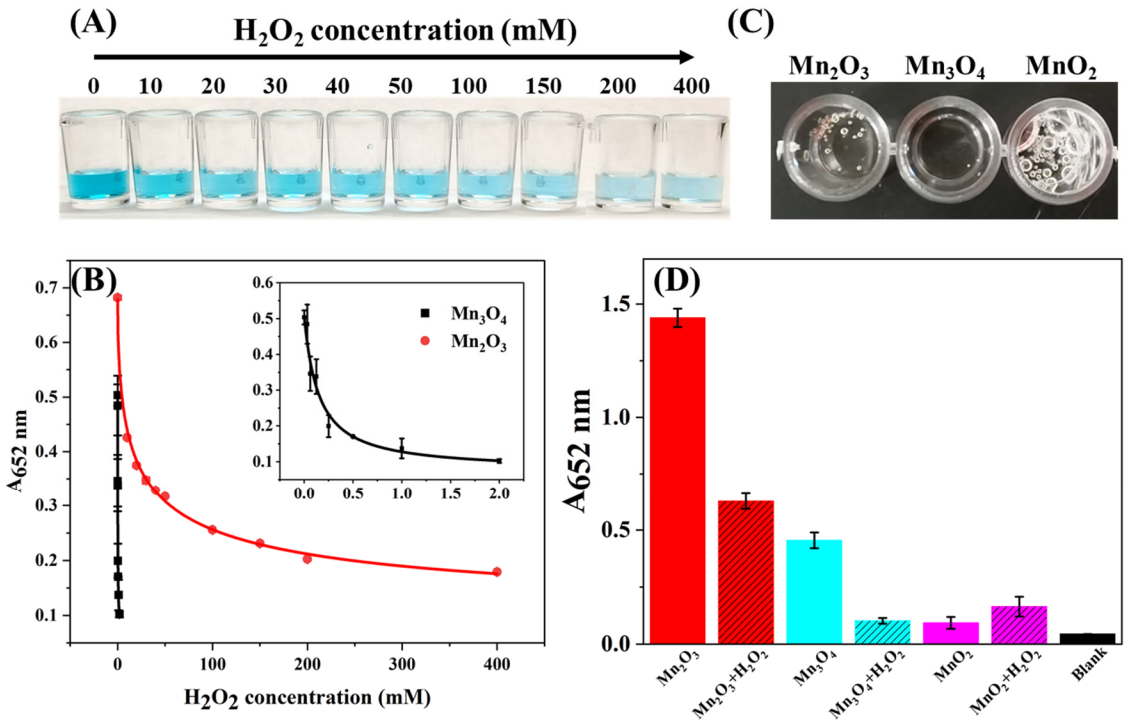

Figure 4. (A) Photographs showing the effect of H_2O_2 on activity of Mn_2O_3 (10 μg/mL)

with 0.5 mM TMB. (B) Quantitative measurement of the absorbance with Mn_2O_3 and Mn_3O_4. Inset: the Mn_3O_4 data. (C) Photographs showing the catalytic activity of the manganese oxides (10 μg/mL) to decompose H_2O_2 (200 mM, in 50 mM pH 4.0 acetate buffer). (D) Activities of the three manganese oxides for oxidation of TMB (0.5 mM, in 50 mM pH 4.0 acetate buffer) in the absence and presence of 20 mM H_2O_2.

Robust Mn_2O_3 oxidase-like activity in the presence of proteins

To use Mn_2O_3 in immunoassays, it is critical to understand the activity in the presence of proteins. While physisorption is a simple method for antibody labeling,[13, 42, 43] protein capping might inhibit nanozyme activities.[44, 45] Herein, we measured the activity of various metal oxides in the presence of BSA. Decreased activity with increase of BSA concentration was observed for all the nanozymes, but Mn_2O_3 was the least inhibited (Figure 5A, B). Therefore, Mn_2O_3 has an excellent potential for immunoassays. We have also examined the inhibition of a few peroxidase-mimicking nanozymes (Figure 5C), and various degrees of inhibition were also observed.

10.1002/chem.202100567

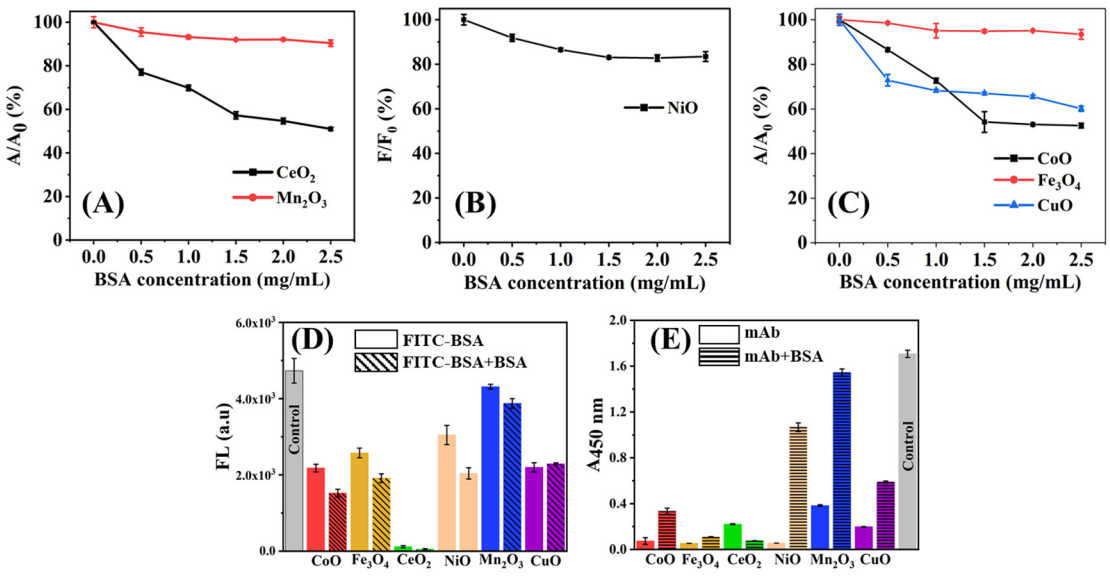

Figure 5. The effect of adsorbed BSA on the oxidase-like activity of (A) CeO_2 and Mn_2O_3; (B) NiO; and (C) nanozymes with peroxidase-like activities (10 mM H_2O_2). A_0 and F_0 are the mean absorbance or florescence without BSA; A or F are the mean absorbance or florescence with BSA. (D) Supernatant fluorescence of FITC-BSA mixed with various metal oxides after centrifugation (solid bars), and adding BSA to FITC-BSA-capped nanozymes (shaded bars). (E) A similar adsorption experiment using a mAb. The mAb was first adsorbed by the oxides and the titer of the supernatant after adding BSA and centrifugation was measured by icELISA.

Feasibility of using Mn_2O_3 for physisorption-based immunoassays

To evaluate protein adsorption by nanozymes, FITC-labeled BSA was mixed with each nanozyme for 30 min adsorption. The mixtures were then centrifuged and the fluorescence

intensity of the supernatants was measured. Most oxides adsorbed more than half of the FITC-BSA, the best adsorption was achieved by CeO_2, while the least adsorption was by Mn_2O_3 (Figure 5D, solid bars). Such capacity difference can be partially attributed to the difference in surface area of the metal oxides. We further added a high concentration of non-labeled BSA to displace pre-adsorbed FITC-BSA, but no replacement was observed for any of the oxides (Figure 5D, shaded bars), indicating that FITC-BSA was stably adsorbed by all.

Such stable physisorption and retained activity in BSA for Mn_2O_3 encouraged us to further test the adsorption of antibodies. We used an anti-ISO mAb for the same protein adsorption test and the concentration of the antibody in supernatant was measured by ELISA (Figure 5E). The protein-adsorption ability of the Mn_2O_3 was still the weakest. However, the adsorbed antibody can be replaced by BSA, and the antibody on Mn_2O_3 was almost fully desorbed. Since BSA is commonly used to blocked non-specificity binding sites after antibody labeling, if antibodies can be replaced by BSA, physisorption for Mn_2O_3 labeling would unlikely to be feasible.

Covalent antibody conjugation

Since physisorption was infeasible for antibody labeling on Mn_2O_3, a covalent conjugation method was applied. Herein, Mn_2O_3 was reacted with 3-aminopropyltriethoxysilanea (APTES), and subsequently conjugated to the antibody via glutaraldehyde (Figure 6A).[21]

The TEM micrograph did not show a full and well-defined shell (Figure 6B), and the EDS data (Figure 6C) showed silicon signal, indicating that APTES might formed a partial layer on the surface. This synthesized Mn_2O_3@APTES was further covalent conjugated to mAb by glutaraldehyde (Figure 6A).

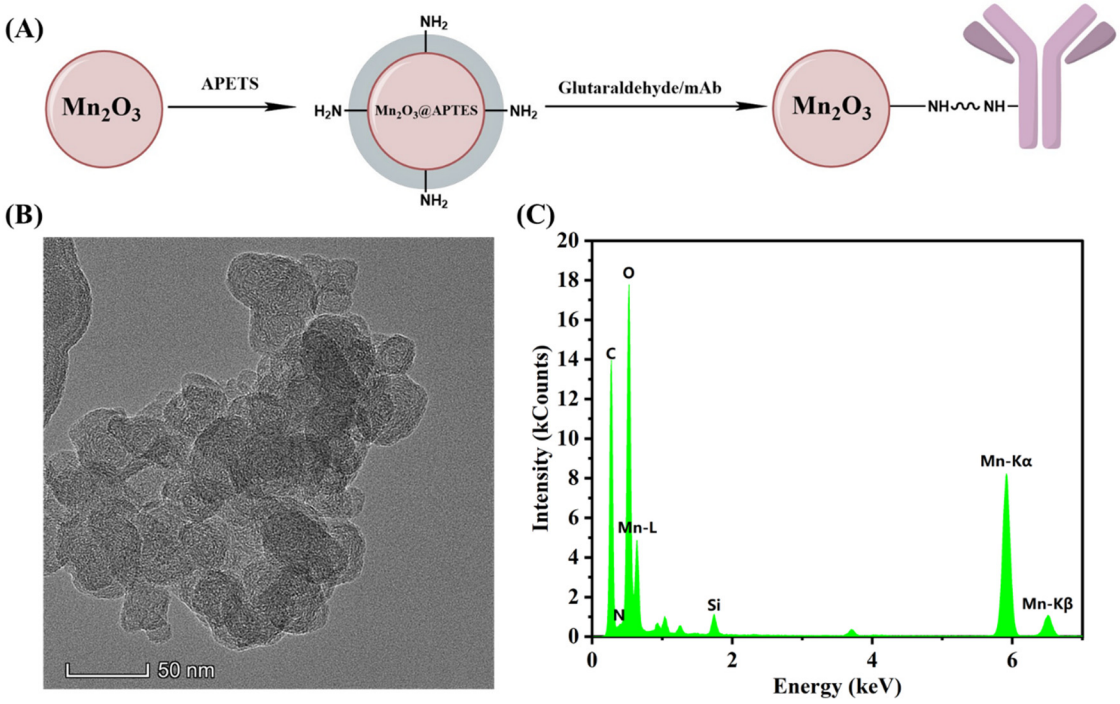

Figure 6. (A) Scheme of Mn_2O_3@APTES conjugation to an antibody. (B) TEM and (C) EDS elemental mapping of Mn_2O_3@APTES.

Immunoassays

The anti-ISO mAb was covalently conjugated by using glutaraldehyde as a crosslinker (Figure 6A). The Mn_2O_3@APTES conjugated mAb achieved obvious titer, indicating that

the mAb was successfully linked to the Mn_2O_3 (Figure S10). Since our target, isocarbophos is a small molecule, a one-step icELISA was used as show in Figure 7B. For developing the one-step icELISA, instead of PBS, 50 μL of serial diluted isocarbophos was applied to create a calibration curve. After washing away the free mAb conjugates, we added a final concentration of 1 mM TMB in 50 mM pH 4.0 acetate buffer for 10 min incubation. The absorbance at 450 nm was measured after adding 50 μL of 10% H_2SO_4. Finally, the anti-isocarbophos calibration curve of two-step icELISA using HRP-labeled secondary antibody for signal generation was also measured for comparison. The 50% decrease in maximum absorbance (IC_{50}) of the one-step icELISA was 261.7 ng/mL, which was higher than that of two-step icELISA (184.7 ng/mL), while the limit of detection (LOD, IC_{10}, 20.4 ng/mL) was lower and the linear range (IC_{20}~IC_{80},52.3~1309.6 ng/mL) was broader (Figure 7C). We then studied the cross-reactivity (CR, %) to evaluate the specificity of the developed one-step icELISA. Negligible CR was observed for all the analogues (Figure 7D), indicating that the developed one-step icELISA was feasible for analytical detection.

We further studied the matrix effect on the one-step icELISA and the results are summarized in Table 1. The recoveries were 92.9%~119.2% and the coefficients of variation (CV) were 4.5%~16.4%. The good recoveries indicated that the developed icELISA can be used for practical samples screening.

10.1002/chem.202100567

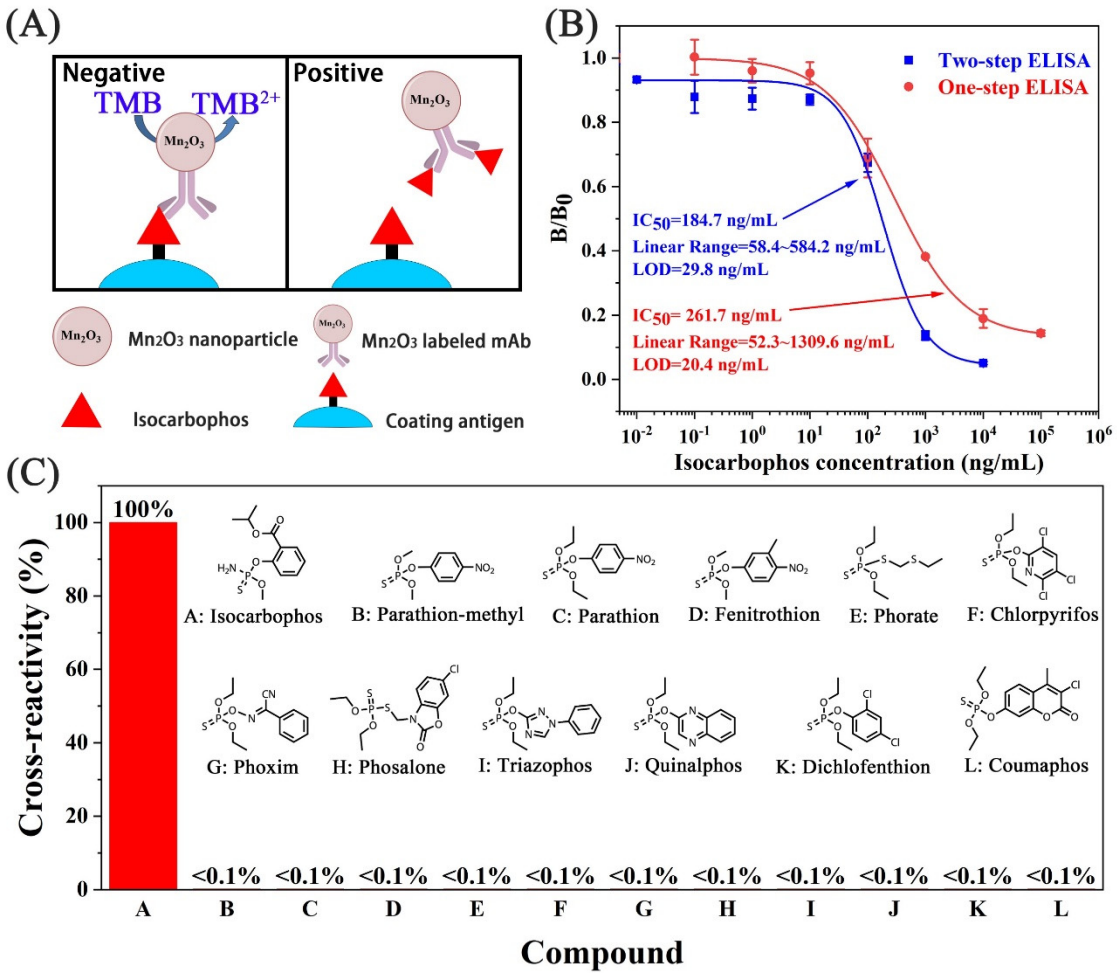

Figure 7. (A) Scheme of Mn_2O_3@APTES conjugation to mAb and its application for the one-step icELISA. (B) The anti-isocarbophos calibration curve of two-step icELISA and one-step icELISA. (D) the cross-reactivity (CR, %) of one-step icELISA. The CR was calculated using CR(%) = [IC_{50} (isocarbophos, ng/mL)/IC_{50} (analogue, ng/mL)]×100.

Table 1. Recoveries of isocarbophos from spiked samples by one-step icELISA (n = 3)[a]

sample	Spiked (ng/mL)	Mean (ng/mL) (mean±SD[b])	Recovery (%)	CV[c] (%)
Cucumber	0[d]	ND[e]	-	-
	1000	998±113	99.8	11.3
	200	221±24	110.5	10.9
	100	119±6	119	5.0
Chinese cabbage	0	ND	-	-
	1000	1089±49	108.9	4.5
	200	202±22	101	10.9
	100	93±15	93	16.1

[a]For one concentration, three positive samples were spiked and determined by ELISA and GC; [b]SD, standard deviation; [c]CV, coefficient of variance, which was obtained from intra-assay; [d]Blank control; [e]ND, not detected.

Conclusions

In summary, we found that Mn_2O_3 had the highest oxidase-like activity among the common manganese oxide nanoparticles. In addition, its activity is also much higher than other metal oxides, including CeO_2 plus F^-. Mn_2O_3 can oxidize a broad range of substrates to produce colorimetric and fluorescent signals. Therefore, Mn_2O_3 is the most efficient and

general oxidase-mimicking metal oxide known so far. Its activity was not much affected by protein adsorption, although its physisorption of antibodies was weak. A covalent conjugation method was developed for antibody labeling by first coating the Mn_2O_3 with an amine-containing silane and subsequently conjugating to antibody by glutaraldehyde. Finally, a one-step icELISA was developed for highly sensitive and selective isocarbophos detection. This Mn_2O_3 nanozyme will find applications in nano and analytical science due to its high efficiency, low-cost, and high stability.

Acknowledgements

Funding for this work is from the Natural Sciences and Engineering Research Council of Canada (NSERC), the Key Project of Guangdong Provincial University of China (2019KJDXM002) and Guangdong Special Support Program of China (2019TX05N052). Z. J. Chen was supported by a China Scholarship Council (CSC) Scholarship to visit the University of Waterloo.

Conflict of interest

The authors declare no conflict of interest.

References

[1] X. Q. Tao, X. Wang, B. W. Liu, J. W. Liu, *Biosens. Bioelectron.* **2020**, *168*, 112537.

[2] J. J. X. Wu, X. Y. Wang, Q. Wang, Z. P. Lou, S. R. Li, Y. Y. Zhu, L. Qin, H. Wei, *Chem. Soc. Rev.* **2019**, *48*, 1004-1076.

[3] Y. Zhou, B. Liu, R. Yang, J. Liu, *Bioconjugate Chem.* **2017**, *28*, 2903-2909.

[4] Y. Huang, J. Ren, X. Qu, *Chem. Rev.* **2019**, *119*, 4357-4412.

[5] J. R. Li, J. Wang, Y. L. Wang, M. Trau, *Analyst* **2017**, *142*, 4788-4793.

[6] F. Q. Yu, Y. Z. Huang, A. J. Cole, V. C. Yang, *Biomaterials* **2009**, *30*, 4716-4722.

[7] B. W. Liu, J. W. Liu, *Nanoscale* **2015**, *7*, 13831-13835.

[8] Y. J. Long, Y. F. Li, Y. Liu, J. J. Zheng, J. Tang, C. Z. Huang, *Chem. Commun.* **2011**, *47*, 11939-11941.

[9] D. M. Duan, K. L. Fan, D. X. Zhang, S. G. Tan, M. F. Liang, Y. Liu, J. L. Zhang, P. H. Zhang, W. Liu, X. G. Qiu, G. P. Kobinger, G. F. Gao, X. Y. Yan, *Biosens. Bioelectron.* **2015**, *74*, 134-141.

[10] M. A. Woo, M. Kim, J. Jung, K. Park, T. Seo, H. Park, *Int. J. Mol. Sci.* **2013**, *14*, 9999-10014.

[11] X. F. Tan, L. H. Zhang, Q. R. Tang, G. X. Zheng, H. Li, *Mikrochim. Acta* **2019**, *186*, 280.

[12] N. Cheng, Y. Song, M. M. A. Zeinhom, Y. C. Chang, L. Sheng, H. L. Li, D. Du, L.

Li, M. J. Zhu, Y. B. Luo, W. T. Xu, Y. H. Lin, *ACS Appl. Mater. Inter.* **2017**, *9*, 40671-40680.

[13] Y. T. Zhao, M. M. Yang, Q. Q. Fu, H. Ouyang, W. Wen, Y. Song, C. Z. Zhu, Y. H. Lin, D. Du, *Anal. Chem.* **2018**, *90*, 7391-7398.

[14] Y. Nangia, B. Kumar, J. Kaushal, C. Raman Suri, *Anal. Chim. Acta* **2012**, *751*, 140-145.

[15] L. Jiao, L. H. Zhang, W. W. Du, H. Li, D. Y. Yang, C. Z. Zhu, *Nanoscale* **2018**, *10*, 21893-21897.

[16] H. Ou Yang, Q. Lu, W. W. Wang, Y. Song, X. M. Tu, C. Z. Zhu, J. N. Smith, D. Du, Z. F. Fu, Y. H. Lin, *Anal. Chem.* **2018**, *90*, 5147-5152.

[17] Y. W. Wang, T. T. Liu, J. W. Liu, *ACS Appl. Nano Mater.* **2019**, *3*, 842-849.

[18] Y. W. Wang, J. Z. Yang, Y. L. Zhao, J. W. Liu, *Chem. Commun.* **2019**, *55*, 13434-13437.

[19] B. W. Liu, Z. C. Huang, J. W. Liu, *Nanoscale* **2016**, *8*, 13562-13567.

[20] M. Liu, Z. H. Li, Y. X. Li, J. J. Chen, Q. Yuan, *Chinese Chem. Lett.* **2019**, *30*, 1009-1012.

[21] Z. J. Chen, Z. C. Huang, S. Huang, J. L. Zhao, Y. M. Sun, Z. L. Xu, J. W. Liu, *Analyst* **2020**.

[22] E. Z. Sheng, Y. X. Lu, Y. T. Tan, Y. Xiao, Z. X. Li, Z. H. Dai, *Food Chem.* **2020**, *331*,

127090.

[23] F. Tian, J. Zhou, B. Jiao, Y. He, *Nanoscale* **2019**, *11*, 9547-9555.

[24] J. Wang, J. Wang, P. Zhou, H. Tao, X. Wang, Y. Wu, *Mikrochim. Acta* **2020**, *187*, 99.

[25] J. Q. Xi, C. H. Zhu, Y. Q. Wang, Q. N. Zhang, L. Fan, *RSC Adv.* **2019**, *9*, 16509-16514.

[26] X. D. Zhang, X. X. Mao, S. Li, W. F. Dong, Y. M. Huang, *Sensor. Actuat. B- Chem.* **2018**, *258*, 80-87.

[27] N. Singh, M. A. Savanur, S. Srivastava, P. D'Silva, G. Mugesh, *Angew. Chem. Int. Edit.* **2017**, *56*, 14267-14271.

[28] G. Mohseni, M. Negahdary, H. Faramarzi, S. Mehrtashfar, A. Habibi-Tamijani, S. H. Nazemi, Z. Morshedtalab, M. Mazdapour, S. Parsania, *Int. J. Electrochem. Sci.* **2012**, *7*, 12098-12109.

[29] Z. W. Kang, R. K. Kankala, B. Q. Chen, C. P. Fu, S. B. Wang, A. Z. Chen, *ACS Appl. Mater. Inter.* **2019**, *11*, 28781-28790.

[30] S. Xiong, Y. C. Deng, Y. Y. Zhou, D. X. Gong, Y. Z. Xu, L. H. Yang, H. H. Chen, L. Chen, T. W. Song, A. Luo, X. L. Deng, C. Y. Zhang, Z. Y. Jiang, *Anal. Methods* **2018**, *1*, 5468-5479.

[31] J. C. Johnson, J. M. Van Emon, D. R. Pullman, K. R. Keeper, *J. Agric. Food Chem.* **1998**, *46*, 3116-3123.

[32] Y. L. Xu, F. Y. Li, F. Ndikuryayo, W. C. Yang, H. M. Wang, *Sensors* **2018**, *18*, 4281.

[33] C. Yu, D. Hao, Q. Chu, T. Wang, S. Liu, T. Lan, F. Wang, C. Pan, *Food Chem.* **2020**, *321*, 126657.

[34] A. Masiá, C. Blasco, Y. Picó, *Trends Environ. Anal. Chem.* **2014**, *2*, 11-24.

[35] J. W. Wong, M. K. Hennessy, D. G. Hayward, A. J. Krynitsky, I. Cassias, F. J. Schenck, *J. Agric. Food Chem.* **2007**, *55*, 1117-1128.

[36] X. R. Wang, Y. Y. Wang, Y. D. Wang, Q. Chen, X. Liu, *Spectrochim. Acta A* **2020**, *226*, 117617.

[37] H. Inui, T. Takeuchi, A. Uesugi, F. Doi, M. Takai, K. Nishi, S. Miyake, H. Ohkawa, *J. Agric. Food Chem.* **2012**, *60*, 1605-1612.

[38] J. J. Zhou, M. S. Ren, W. J. Wang, L. Huang, Z. C. Lu, Z. Y. Song, M. F. Foda, L. Zhao, H. Y. Han, *Anal. Chem.* **2020**, *92*, 8802-8809.

[39] Y. Z. Liu, G. X. Zhao, P. Wang, J. Liu, H. C. Zhang, J. P. Wang, *J. Environ. Sci. Heal. B* **2013**, *48*, 139-146.

[40] Y. Li, L. Q. Liu, H. Kuang, C. L. Xu, *Food Chem.* **2020**, *311*.

[41] J. Y. Zhang, S. H. Wu, X. M. Lu, P. Wu, J. W. Liu, *Nano Lett.* **2019**, *19*, 3214-3220.

[42] Z. Q. Gao, M. D. Xu, L. Hou, G. N. Chen, D. P. Tang, *Anal. Chim. Acta* **2013**, *776*, 79-86.

[43] J. S. Lin, D. P. Tang, *Anal. Methods* **2016**, *8*, 4069-4074.

[44] R. Pautler, E. Y. Kelly, P. J. Huang, J. Cao, B. Liu, J. Liu, *ACS Appl. Mater. Inter.* **2013**, *5*, 6820-6825.

[45] N. J. Lang, B. W. Liu, J. W. Liu, *J. Colloid. Interf. Sci.* **2014**, *428*, 78-83.

Graphical abstract

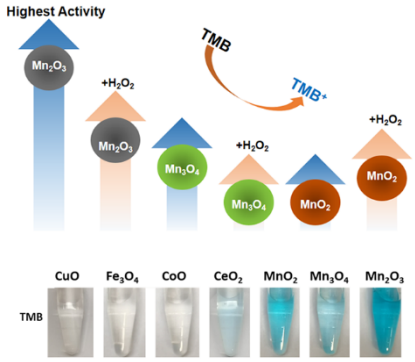

Mn_2O_3 nanoparticles have the highest oxidase-like nanozyme activity among the tested metal oxides, but its activity is inhibited by H_2O_2. Mn_3O_4 behaves similarly, while the activity of MnO_2 is enhanced by H_2O_2. After coating the Mn_2O_3 nanoparticles with an amine-containing silane, covalent conjugation to antibodies is achieved for the highly sensitive and selective detection of isocarbophos using an immunoassay.